Forestry Research Advances

ARTICLE

Open Access

https://doi.org/10.48130/fra-0026-0005

Forestry Research Advances **2026**, 1: e008

Pericarp thickness formation and *CdCSE4*-mediated lignin accumulation during *Camellia drupifera* fruit development

Yang Shen[#], Boyong Liao[#*], Wanyu Xiong, Shan He, Hongjian Shen, Yongjuan Li, Bipei Zhang and Yongquan Li[*]

College of Horticulture and Landscape Architecture, Zhongkai University of Agriculture and Engineering, Guangzhou 510225, China

[#] Authors contributed equally: Yang Shen, Boyong Liao

[*] Correspondence: liaoby05@zhku.edu.cn (Liao B); yongquanli@zhku.edu.cn (Li Y)

Abstract

Pericarp thickness is a crucial agronomic trait that influences the seed yield ratio and overall productivity of *Camellia drupifera*. However, the structural basis and regulatory mechanisms governing the deposition of cell wall components during pericarp thickening remain unclear. In this study, morphological, biochemical, and molecular comparisons were conducted between thick-pericarp (HP) and thin-pericarp (TP) fruits. The results demonstrated that HP had a significantly greater proportion of pericarp and higher lignin content than TP, whereas its seed yield per fruit was significantly lower. Histological analyses revealed thicker cell walls, higher levels of lignification, and more fully developed sclereids in the thicker pericarp. Correlation analysis demonstrated a significant positive relationship between lignin content and pericarp thickness. Caffeoyl shikimate esterase (CSE) is a key hydrolase in the lignin biosynthetic pathway. Gene family analysis identified 17 *CdCSE* genes, which are highly conserved in the areas of domain architecture and physicochemical properties. Expression profiling confirmed that *CdCSE4* was highly expressed in HP and was strongly associated with lignin accumulation. Heterologous expression assays demonstrated that *CdCSE4* positively regulates lignin biosynthesis and successfully restores the wild-type phenotype in the *cse* mutant of *Arabidopsis thaliana*, significantly increasing lignin monomer content and altering the monomeric composition. Taken together, these findings demonstrate that *CdCSE4* promotes pericarp lignification by modulating the lignin biosynthetic pathway, thereby potentially influencing the development of pericarp thickness. This study provides theoretical insights and valuable genetic resources for elucidating the molecular mechanisms of pericarp development and improving fruit quality in *C. drupifera*.

Keywords: Camellia drupifera, Pericarp thickness, Lignin, CSE gene family

Citation: Shen Y, Liao B, Xiong W, He S, Shen H, et al. 2026. Pericarp thickness formation and *CdCSE4*-mediated lignin accumulation during *Camellia drupifera* fruit development. *Forestry Research Advances* 1: e008 https://doi.org/10.48130/fra-0026-0005

Introduction

Extensively cultivated across southern China, *C. drupifera* is a highly productive, large-fruited germplasm resource of seed-oil camellia. Analysis of the seed kernel oil reveals a predominant unsaturated fatty acid content (82.72%–88.01%), alongside substantial quantities of functional biomolecules, specifically squalene and phytosterols[1,2]. However, *C. drupifera* exhibits considerable variation in its fruit traits[3,4]. Excessive pericarp thickness often leads to a reduced seed yield ratio, which has become one of the major constraints on its large-scale cultivation. Phenotypic variance in pericarp thickness substantially exceeds the fluctuations observed in fresh seed yield, fruit length, and overall diameter, as documented in earlier investigations[5,6], suggesting that this trait possesses significant potential for genetic improvement and selective breeding. Our previous survey of *C. drupifera* germplasm resources in Huizhou[7], Guangdong Province, revealed a broad spectrum of pericarp measurements (2.25–41.50 mm), alongside a robust inverse association with fresh seed yield. Our results therefore highlight pericarp depth as a principal bottleneck restricting overall fruit yield in *C. drupifera*. Nevertheless, the precise mechanisms driving pericarp thickening in *C. drupifera* remain obscure.

The expansion of the pericarp is heavily dependent on the differentiation of sclereids alongside secondary cell wall deposition. This architectural fortification necessitates the large-scale production and subsequent cross-linking of key structural biopolymers, specifically lignin, cellulose, and hemicellulosic matrices[8]. Within *Capsicum annuum* germplasm, variants possessing a thinner pericarp typically accumulate greater concentrations of hemicellulosic polymers, cellulose, and pectin than their thicker-walled counterparts[9]. In *Camellia* species, thick-pericarp materials generally have higher lignin contents, accompanied by a significant upregulation of S-lignin monomers[10]. Lignin deposition results in cell wall thickening and sclereid formation, maintaining the structural stability of the pericarp[11,12]. Although the regulation of pericarp lignification and sclereid formation has been explored in other woody fruits such as *Pyrus ussuriensis*[13,14], the mechanisms underlying pericarp lignification and its regulatory network within *C. drupifera* remain largely unknown, limiting the molecular improvement of pericarp-related traits in breeding programmes.

As a fundamental divergence from general phenylpropanoid metabolism, the biosynthesis of lignin is orchestrated by a complex network of critical enzymes[15]. Among them, caffeoyl shikimate esterase (CSE) is a crucial hydrolase that catalyzes the conversion of caffeoyl shikimate (3-CQA) into caffeic acid (CA), thereby regulating monolignol flux and the overall lignification level[16]. Thus far, homologs belonging to the *CSE* family have been comprehensively characterized in *Arabidopsis thaliana*, *Medicago sativa*, *Pyrus bretschneideri*, cucumber (*Cucumis sativus)*, tomato (*Solanum lycopersicum*), and *Populus trichocarpa*, with 16, 2, 24, 8, 11, and 18 genes, respectively[17–22]. Functional studies have demonstrated that *CSE* genes in *A. thaliana*, poplar (*Populus* spp.), *Petunia*, and pear (*Pyrus* spp.) are essential for lignification, phenylpropanoid metabolism, and carbohydrate synthesis. For instance, in cucumber, *CsCSE5* positively regulates resistance to fungal pathogens (*Podosphaera xanthii* and *Corynespora cassiicola*), whereas *CsCSE1* modulates the

https://doi.org/10.48130/fra-0026-0005

expression of downstream lignin-related genes (*CsLACs*, *CsCOMTs*, *CsCCRs*, and *CsCADs*), thereby mediating disease resistance[21]. Similarly, *SlCSE6* in tomato promotes lignin deposition and enhances resistance to *Botrytis cinerea* infection[22]. However, no systematic identification or functional characterization of the *CSE* gene family has yet been reported in *C. drupifera*.

In this study, *C. drupifera* was used as the research material to investigate differences in pericarp structure, cell wall components, and lignification between the thick-pericarp (HP) and thin-pericarp (TP) types. On the basis of transcriptomic data, the *CSE* gene family was identified and characterized in *C. drupifera* to explore its potential roles in pericarp lignification. Functional validation was performed in transgenic *A. thaliana* to examine the genes' functions in lignin biosynthesis. This research yields profound insights into the molecular processes driving pericarp development, while delivering valuable genetic resources to enhance fruit traits in *C. drupifera*.

Materials and methods

Plant materials and sample preparation

Two cultivated varieties of *C. drupifera* that naturally exhibit significantly different pericarp phenotypes (the HP type and the TP type) were selected from our germplasm resource base. Clonal plants obtained from these two specific varieties via vegetative propagation were used for all experiments. All sampled trees were of the same age and grown naturally in Huizhou, Guangdong Province, under similar environmental conditions. To accurately capture the rapid developmental changes and the subsequent stable maturation phase, fruits were sampled biweekly during the early stages (78, 92, 105, 124, 139, 154, and 168 d after bloom [DAB, hereafter denoted as d]) and monthly during the later stages (200, 231, 263, 291, and 311 d). At each time point, three biological replicates were obtained, each comprising at least five fruits of uniform size and developmental stage. After being excised directly in the field, the pericarp samples were rapidly quenched in liquid nitrogen and brought to the laboratory. These tissues were kept at −80 °C until required for RNA extraction and the quantification of cell wall components. Tissue segments from the equatorial region of the fruit were fixed in 2.5% glutaraldehyde and a formaldehyde–acetic acid (FAA) solution comprising 70% ethanol:formaldehyde:acetic acid at 90:5:5 (v/v/v) at 4 °C for transmission electron microscopy and paraffin sectioning, respectively.

Phenotypic trait measurements

At each developmental stage, the following fruit traits were measured: Fresh fruit weight (g), transverse and longitudinal diameters (mm), pericarp thickness (mm), moisture content (%), and pericarp proportion (%). A YP3002 electronic balance was used to quantify the fresh mass of the fruits immediately upon collection (Youke Instruments, China). The maximum transverse and longitudinal diameters were measured using a GREENER digital vernier caliper. Pericarp thickness was determined along the equatorial section of the fruit using the same caliper. Pericarp moisture content (%) was calculated as [(Fresh weight − Dry weight)/Fresh weight] × 100. Pericarp proportion (%) was calculated as (Pericarp fresh weight/Fruit fresh weight) × 100. Cross-sections of the fruits were photographed using a Canon EOS 200D II camera before and after staining with a phloroglucinol–HCl solution (prepared by dissolving 2 g of phloroglucinol in 100 mL of absolute ethanol and mixing thoroughly with 40 mL of concentrated hydrochloric acid) for 5 min[23]. The light source and exposure conditions were kept constant during imaging.

Preparation of pericarp sections and microscopic observation

To prepare for paraffin embedding, the FAA-fixed samples were processed through a progressive ethanol gradient for complete moisture removal, followed by xylene treatment for tissue clearing. Sections (8–10 μm thick) were cut using a rotary microtome (Leica RM2255, Germany), stained with safranin, and examined under a Leica DM750 optical microscope. For the quantification of cell wall thickness, scanned paraffin sections were analyzed using SlideViewer 2.5 software. For each pericarp type, 50 independent measurements were obtained by randomly selecting five regions and taking 10 measurements per region. For targeted structural examinations, freehand sections were generated from the stabilized pericarp specimens and subsequently stained with a phloroglucinol–HCl mixture for 5 min. The sections were observed and imaged under a Leica EZ4 W stereomicroscope. All micrographs were taken under identical illumination conditions.

Scanning electron microscopy and energy-dispersive spectroscopy analysis

Small pericarp sections were sequentially immersed in 2.5% glutaraldehyde and 1% osmium tetroxide. After dehydration with increasing ethanol concentrations, the tissues were dried in a critical-point apparatus. The dehydrated samples were then mounted onto aluminum bases with carbon tape and sputter-coated with a conductive gold layer (45 s, 10 mA) utilizing a Quorum SC7620 unit. A TESCAN MIRA LMS scanning electron microscope, fitted with an SE2 detector, was deployed for morphological and elemental assessments. The beam energies were specifically adjusted to 3 kV for high-resolution surface imaging and 15 kV for energy-dispersive X-ray spectroscopy (EDS) spectral mapping, with all visual data subsequently saved for analysis.

Determination of lignin, cellulose, and hemicellulose contents

Lignin content: Lignin content was determined following the method of Lin et al.[24], with minor modifications. Dried and ground samples (approximately 3 mg) were subjected to acetylation, water bath incubation, and centrifugation. The absorbance was measured at 280 nm using a SpectraMax Mini microplate reader, and the lignin content (mg g^{-1}) was calculated as Lignin content (mg g^{-1}) = $1.4561 \times \Delta A / W$, where $\Delta A = A_{measured} - A_{blank}$, and W represents the sample weight. Cellulose content: For the determination of cellulose content, approximately 0.3 g of each dried sample was treated with ethanol–acetone to remove impurities, hydrolyzed with sulfuric acid, and reacted with a chromogenic reagent. The absorbance was read at 620 nm, and the cellulose content (mg g^{-1}) was calculated from a standard calibration curve. Hemicellulose content: For determining the hemicellulose content, about 0.05 g of each dried sample was treated with ethanol, extracted, and reacted with a chromogenic reagent. The absorbance was recorded at 540 nm, and the hemicellulose content (mg g^{-1}) was quantified according to a standard xylose calibration curve.

Determination of lignin monomercomposition

Evaluation of the lignin monomers relied on the gas chromatography–mass spectroscopy (GC–MS) procedures outlined by[25].

Desiccated pericarps (100 mg) were hydrolyzed in sealed vials containing 2 mL of 4 mol L^{-1} NaOH at 95 °C for 24 h. Upon cooling, samples were neutralized with 1.6 mL of 6 mol L^{-1} HCl and centrifuged (13,000 rpm, 5 min). Two successive 1-mL ethyl acetate extractions were performed on 500 μL of the resulting supernatant. Nitrogen-dried organic phases were taken up in 1 mL of methanol and filtered (0.45 μm) prior to triplicate GC–MS analyses. Analytes were resolved on an RTX-5MS column (30 m × 0.25 mm × 0.25 μm) with a helium flow of 1.17 mL min^{-1}. Operational parameters included a 250 °C injection port (10:1 split), a 200 °C ion source, and a 250 °C interface. Data acquisition covered a 32–200 m/z range after a 3-min solvent delay, with the final contents calculated via authentic standard curves.

Identification and analysis of the *CSE* gene family

The identification of the *CSE* gene family was based on previously reported *A. thaliana* (At1g52760) and *P. trichocarpa*[20] protein sequences. The genome files of *P. trichocarpa* and *A. thaliana* were downloaded from the TAIR (www.arabidopsis.org) and Phytozome (https://phytozome-next.jgi.doe.gov) databases (accessed on 20 October 2025)[26].

The AtCSE protein sequence was used as a query to perform BLASTP searches (E-value ≤ 1×10^{-5}) for homologous proteins. To improve accuracy, HMMER v3.3.2 (www.ebi.ac.uk/interpro/entry/pfam/#table, accessed on 20 October 2025) was used to identify candidate genes on the basis of the conserved Pfam domain PF12146 of the haloacid dehalogenase (HAD)-like family. The BLAST and Hidden Markov Model (HMM) results were integrated, and candidate sequences were further verified through Pfam[27], Simple Modular Architecture Research Tool (SMART; https://smart.embl-heidelberg.de, accessed on 20 October 2025), and the Conserved Domain Database (CDD; www.ncbi.nlm.nih.gov/cdd, accessed on 20 October 2025) to confirm the presence of the HAD family domain. Given the current lack of a reference genome for *C. drupifera*, its *CSE* genes were identified from transcriptome data assembled using Trinity and manually curated to obtain full-length coding sequences (CDSs). The identified *CdCSE* genes are listed in Supplementary Table S1. The physicochemical properties of the CdCSE proteins were analyzed using TBtools-II[28] software, and the results are provided in Supplementary Table S2.

Phylogenetic analysis of the CSE protein sequences from *A. thaliana*, *P. trichocarpa*, and *C. drupifera* was performed using MEGA v11.0[29]. Phylogenetic trees were constructed using both the neighbor-joining (NJ) and maximum likelihood (ML) methods with 1,000 bootstrap replicates to assess branch reliability. Tree visualization and annotation were conducted using the Interactive Tree of Life (iTOL) online platform (https://itol.embl.de, accessed on 20 October 2025). To investigate the structural characteristics, the secondary structures of the identified CdCSE proteins were predicted using the SOPMA server (https://npsa.lyon.inserm.fr/cgi-bin/npsa_automat.pl?page=/NPSA/npsa_sopma.html, accessed on 20 October 2025). Furthermore, their tertiary structures (three-dimensional [3D] models) were generated by the SWISS-MODEL server (https://swissmodel.expasy.org, accessed on 20 October 2025), based on homology modeling. These structural predictions were conducted to analyze the spatial conformations and folding patterns, which may influence the specific substrate-binding affinities and catalytic activities of the CdCSE proteins.

RNA extraction and expression analysis

Total RNA was isolated from *C. drupifera* pericarps with the Plant Total RNA Extraction Kit (Vazyme, RC411-01, Nanjing, China). Following quality and purity verification via 1% agarose gel electrophoresis and NanoOne spectrophotometry (Yooning, China), 1 μg of RNA was reverse-transcribed into cDNA using the HiScript® III All-in-one RT SuperMix Perfect for qPCR Kit (Vazyme, R333, Nanjing, China). For transcript quantification, quantitative real-time polymerase chain reaction (qRT-PCR) was conducted on a CFX Connect™ Real-Time PCR Detection System (Bio-Rad, USA) utilizing Taq® Pro Universal SYBR qPCR Master Mix (Vazyme, Q712, Nanjing, China). The amplification protocol included primary denaturation at 95 °C for 30 s, followed by 40 cycles consisting of 95 °C for 10 s, 60 °C for 30 s, and 72 °C for 34 s. Expression data were normalized to the *CdGAPDH* internal control, and fold changes were calculated applying the $2^{-\Delta\Delta C_T}$ method. All targeted primer sequences are detailed in Supplementary Table S3.

Vector construction and subcellular localization assay

Specific primers containing the *Kpn*I and *Sal*I restriction sites were designed using CE Design V1.03 software, based on the multiple cloning sites of the pCAMBIA2300-CpYGFP vector. The full-length CDS of *CdCSE4* was amplified using 2× Hieff Canace® Gold PCR Master Mix (YEASEN, Shanghai, China). The polymerase chain reaction (PCR) product was ligated downstream of the CaMV 35S promoter in the pCAMBIA2300-CpYGFP vector using a NovoRec® Plus One-Step Cloning Kit (Novoprotein, China) to generate the recombinant construct pCAMBIA2300-35S::*CdCSE4*. The fusion plasmid was first transformed into *Escherichia coli* strain DH5α (Weidi Bio, China) via the standard heat-shock method. After confirmation of the sequencing (Sangon Biotech, Shanghai, China), the verified construct was subsequently introduced into *Agrobacterium tumefaciens* strain GV3101 via the freeze–thaw method.

For subcellular localization, *Agrobacterium* GV3101 cells carrying either the fusion construct or the empty green fluorescent protein (GFP) vector (control) were infiltrated into *Nicotiana benthamiana* leaves at the four- to five-leaf stage (optical density [OD_{600}] = 0.5). After incubation for 48 h, GFP fluorescence signals were observed and imaged using a confocal laser scanning microscope (FV10-ASW, Olympus, Japan) with an excitation wavelength of 488 nm and an emission detection range of 500–550 nm.

Generation of transgenic *A. thaliana*

Wild-type *A. thaliana* (Col-0) and *cse* T-DNA insertion mutant lines (purchased from the AraShare Technology Service Center, www.arashare.cn) were transformed using the floral dip method. T_1 seeds were screened on Murashige and Skoog (MS) medium supplemented with 50 mg/L kanamycin. Genomic DNA was extracted from resistant seedlings using the cetyltrimethylammonium bromide (CTAB) method, and transgenic plants were confirmed by PCR. Subsequent selection on a kanamycin-containing medium yielded homozygous T_3 transgenic lines. Wild-type and transgenic plants were grown under identical conditions for phenotypic and biochemical analyses.

Statistical analysis

Compilation of the initial dataset and preprocessing were executed within Excel 2024. Quantitative findings are expressed as means accompanied by their respective standard deviations (SDs). Prior to parametric assessments, the Shapiro–Wilk procedure in SPSS v25.0 (IBM, USA) was used to confirm the normality of the distributions. For datasets satisfying this prerequisite, one-way analysis of variance (ANOVA) was applied, supplemented by least

https://doi.org/10.48130/fra-0026-0005

significant difference (LSD) post hoc evaluations to delineate intergroup variations. To explore and graphically represent the interplay among pericarp characteristics, biochemical profiles, and transcript abundances, Pearson correlation matrices were generated via the corrplot package within the R environment (v4.3.1). A two-tailed significance threshold was strictly maintained across all statistical procedures. Final graphical visualizations were constructed by using a combination of Origin 2024, GraphPad Prism 11, and R.

Results

Phenotypic characteristics of HP and TP fruits

Significant morphological differences were observed between HP and TP fruits during development. Transverse sections showed that differences in pericarp thickness became evident from the early developmental stage (139 d), whereas seed kernel development showed little variation between the two types (Fig. 1a). Both fruit types exhibited a typical sigmoidal (S-shaped) growth pattern, with similar longitudinal and transverse diameters. Fruit growth remained slow during the early stage, accelerated after 139 d, and stabilized when the kernel was fully developed at approximately 263 d. The pericarp proportion decreased rapidly at 139 d, indicating that the kernel began to expand rapidly and gradually occupied the pericarp space. However, because of its thicker pericarp, HP maintained a significantly higher proportion of pericarp than TP, indirectly suggesting that pericarp thickness markedly reduces the seed yield ratio. The pericarp moisture content exhibited a typical double-sigmoidal pattern, reaching two peaks at 139 and 263 d. During the early developmental stages, HP showed a higher moisture content than TP, whereas in the later stages, HP exhibited a lower moisture content, indicating a shift in water accumulation dynamics during fruit maturation. Pericarp thickness was the most distinct trait between the two fruit types. HP exhibited a rapid increase in pericarp thickness from 78 to 154 d, reaching the

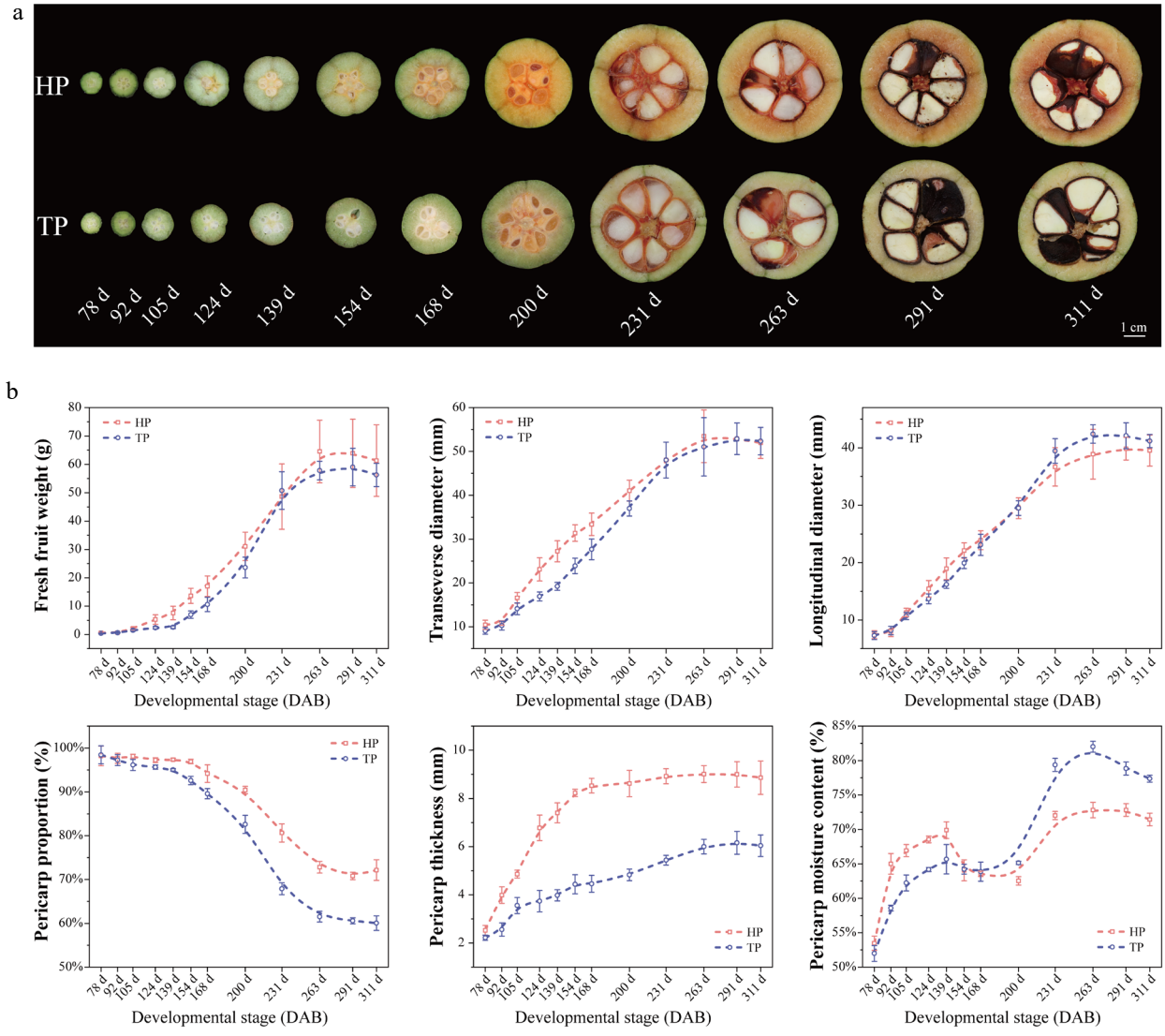

Fig. 1 Morphological characteristics and dynamic changes in the phenotypic traits of HP and TP fruits during development. (a) Representative transverse sections of HP and TP fruits at different developmental stages (78, 92, 105, 124, 139, 154, 168, 200, 231, 263, 291, and 311 d). The HP fruits consistently exhibited a markedly thicker pericarp throughout development. (b) Dynamic changes in the main phenotypic traits of HP and TP fruits during development, including fresh fruit weight (g), transverse diameter (mm), pericarp moisture content (%), proportion of pericarp (%), pericarp thickness (mm), and longitudinal diameter (mm). Data represent the mean ± SD of three biological replicates.

greatest difference from TP at 168 d, whereas TP showed a steady but slower increase throughout the entire developmental period.

Histochemical staining and identifying the developmental stage of the pericarp

To investigate the differences in lignification between HP and TP during fruit development, lignin staining of pericarps at different developmental stages was performed (Fig. 2a, Supplementary Fig. S1). The staining results showed that both HP and TP exhibited distinct lignification features at the early developmental stage, but the extent and timing of lignification differed significantly between the two. Between 124 and 168 d, lignification rapidly progressed from the exocarp towards the endocarp, with HP showing a delayed onset compared with TP. After complete lignification of the pericarp, seed enlargement and nutrient accumulation became evident. By 200 d, lignification had further intensified, as indicated by increased lignin deposition and sclereid formation. At 231 d, the rapid expansion of the seed caused pericarp stretching, leading to a lighter staining intensity per unit of area and elongation of the sclereids. At this stage, the outer seed coat began to lignify; by 263 d, the lignification of the seed coat was complete, though the seed kernel had ceased expanding.

On the basis of the phenotypic data and lignin staining patterns, fruit development was divided into three stages (Fig. 2b). Before 139 d, fruits were in a slow growth stage, then after 231 d, they entered a steady stage. The pericarp's development could be further divided into a thickening stage (characterized by rapid lignification) and an extension stage. Lignification of the pericarp progressed inward, after which the seed began to develop rapidly. When the seed kernel completely filled the seed cavity and the lignification of the seed coat was completed by 263 d, the seed kernel entered a rapid oil accumulation stage.

These results indicate that pericarp thickening is closely associated with the degree of lignification, and that seed kernel development is also correlated with the lignification of both the pericarp and the seed coat.

Histological and ultrastructural features of the pericarp

Paraffin section analysis revealed that HP pericarp cells exhibited a markedly higher degree of lignification, characterized by significantly thickened cell walls and a greater number of elongated sclereids (Fig. 3a). Quantitative analysis confirmed that the cell wall thickness of HP was significantly greater than that of TP (Fig. 3b),

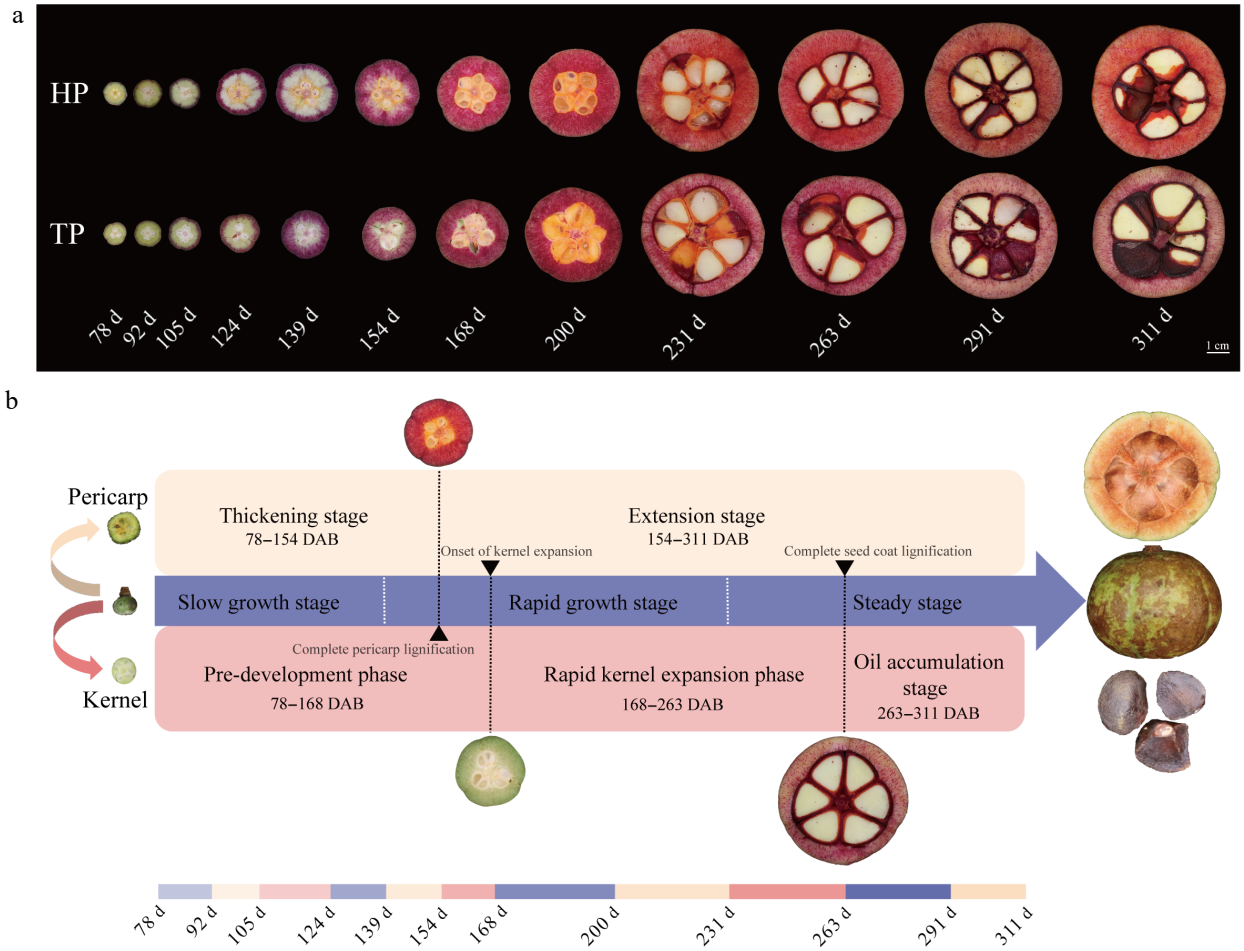

Fig. 2 Lignification patterns of the pericarp in HP and TP fruits and classification of fruit developmental stages. (a) Phloroglucinol–HCl staining of transverse sections of the pericarp from 78 to 311 d, showing progressive lignification from the outer to the inner pericarp. HP pericarps exhibited a deeper lignin staining intensity than TP. (b) Schematic model of *C. drupifera* fruit development. Fruit development was divided into three stages: Slow growth, rapid growth, and steady stage. Pericarp development included a thickening stage (78–154 d) and an extension stage (154–311 d). Seed kernel development was divided into a pre-development phase (78–168 d), a rapid kernel expansion phase (168–263 d), and an oil accumulation stage (263–311 d).

https://doi.org/10.48130/fra-0026-0005

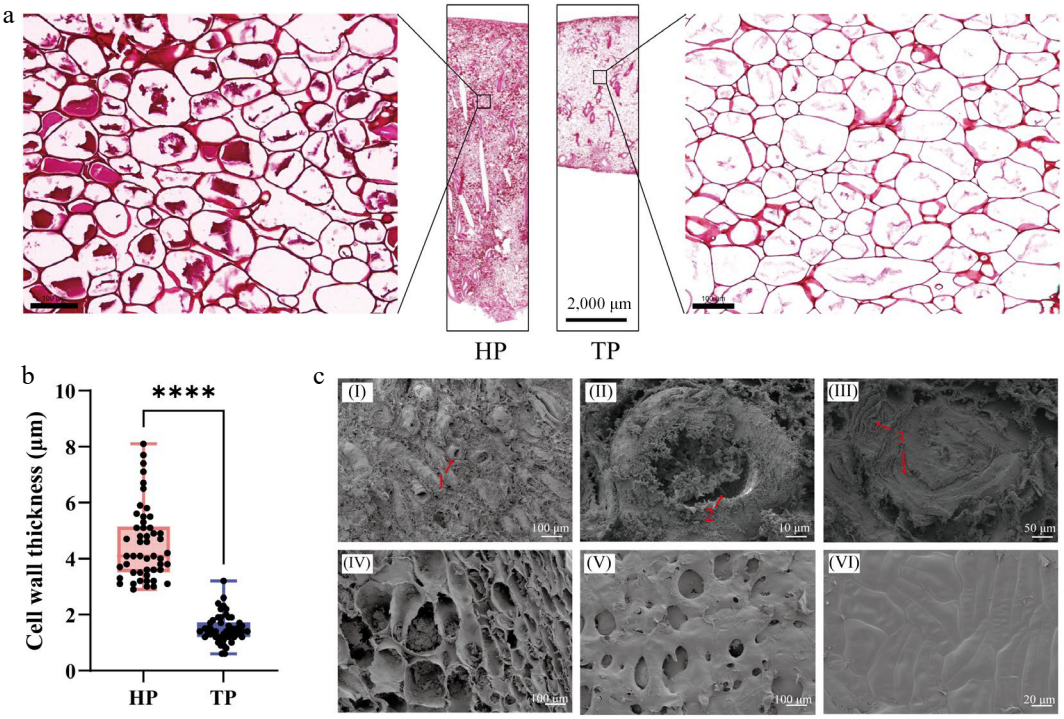

Fig. 3 Anatomical structure and microscopic morphology of the pericarp in HP and TP fruits. (a) Paraffin sections of mature pericarps from HP and TP stained with safranin. The enlarged views show that HP possesses markedly thicker cell walls, whereas TP exhibits thinner walls with a lower degree of lignification. (b) Statistical analysis of cell wall thickness in HP and TP pericarps (n = 50). Asterisks denote a significant difference between HP and TP, based on Student's t-test (**** $p < 0.0001$). (c) SEM images showing the microstructure of the pericarp. (I–III) Morphology and structural characteristics of sclereids; (IV) parenchyma cell structure; (V) inner epidermis; (VI) outer epidermis. Numbered red labels indicate the following: 1, sclereid cells; 2, pits and plasmodesmata on the sclereid wall; 3, lamellar thickening of sclereid cells' secondary walls.

providing an anatomical basis for the thicker pericarp phenotype. In contrast, TP pericarp cells possessed thinner walls, with significantly less dense and smaller sclereids. These histological features are consistent with the TP phenotype, indicating that cell wall thickness and sclereid development are key structural factors influencing pericarp thickness in *C. drupifera*.

Scanning electron microscopy (SEM) observations also revealed that the pericarp comprised multiple compactly arranged cell layers, in which the exocarp, mesocarp, and distinct vascular bundles were clearly distinguished, together with well-developed sclereid clusters. The sclereids showed typical secondary wall thickening with evident lamellar structures, and their inner walls displayed visible pits and plasmodesmata connections. Furthermore, the inner epidermis was distinctly observed, whereas the outer epidermal cells were aligned parallel to the fruit surface and coated with a cuticle and waxy layer, which may contribute to surface protection and reduced water permeability (Fig. 3c). Elemental analysis using EDS (Supplementary Fig. S2) showed that both HP and TP pericarps were mainly composed of carbon (C) and oxygen (O), with identical peak positions and only minor differences in relative intensity. These results suggest that the formation of thicker pericarps in HP is not attributable to differences in elemental composition, but rather to structural modifications in cell wall organization.

Cell wall composition and its correlation with pericarp thickness

To investigate the contribution of major cell wall components to pericarp thickening, the contents of lignin, hemicellulose, and cellulose were quantitatively determined in HP and TP pericarps at different developmental stages, and their relative proportions and correlations with phenotypic traits were analyzed (Fig. 4). The results showed that lignin content in both HP and TP exhibited a dynamic "increase–decrease–stabilize" trend during fruit development. HP pericarps consistently maintained significantly higher lignin levels than TP, reaching over 400 mg/g at maturity (Fig. 4a), indicating that lignin deposition is a key material basis for pericarp thickening. The variation in hemicellulose content was generally consistent with that of lignin, but TP pericarps maintained higher hemicellulose levels throughout development (Fig. 4b). In contrast, cellulose content showed a marked decreasing trend (Fig. 4c): HP pericarps had higher cellulose content with a smaller decline, whereas TP pericarps decreased sharply from approximately 350 mg/g at the early stage to nearly 150 mg/g at maturity, suggesting more pronounced remodeling of the cell wall structure during development.

The relative proportions of the three components revealed further structural differences between the two pericarp types (Fig. 4d, e). In HP, lignin accounted for about 40% of the total wall composition, significantly higher than the ~20% observed in TP. In contrast, TP pericarps contained the highest proportion of hemicellulose (~45%), nearly twice that of HP (~20%). The proportion of cellulose gradually decreased in both types, remaining relatively stable in HP (from 40% to 35%) but dropping dramatically in TP (from ~60% to 23%). Correlation analysis (Fig. 4f) showed that pericarp thickness (PT) was significantly and positively correlated with lignin content (LC) ($r = 0.80$, $p < 0.001$), whereas no significant correlation was observed with hemicellulose content (HC) ($r = 0.35$) or cellulose content (CC) ($r = 0.021$). In summary, the HP phenotype is characterized by increased lignin deposition and significant secondary wall thickening, with lignin content exhibiting a significant positive correlation with pericarp thickness.

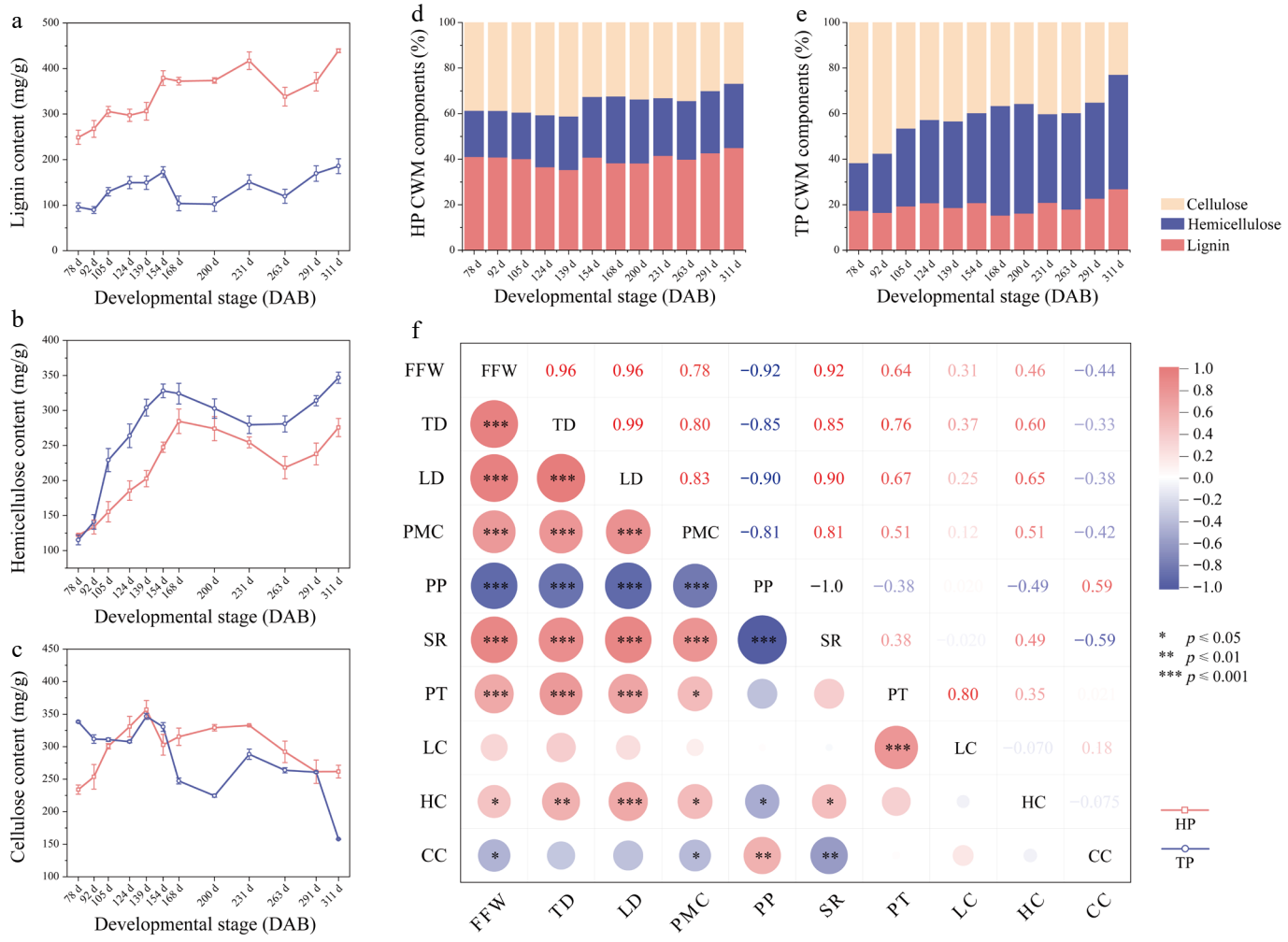

Fig. 4 Analysis of cell wall composition and its correlation with fruit traits in HP and TP pericarps. (a)–(c) Changes in lignin (a), hemicellulose (b), and cellulose (c) contents in HP and TP pericarps at different developmental stages (78–311 d). HP maintained a significantly higher lignin content throughout development, whereas TP exhibited greater accumulation of hemicellulose and cellulose. (d)–(e) Relative proportions of the three major cell wall components—lignin, hemicellulose, and cellulose—in HP (d) and TP (e) pericarps. HP showed a consistently higher proportion of lignin, whereas TP cell walls were dominated by hemicellulose and cellulose. (f) Correlation analysis between cell wall components and fruit phenotypic traits. The color of each circle indicates the correlation direction (red: positive; blue: negative), and circle size reflects the strength of the correlation. Abbreviations: FFW, fresh fruit weight; TD, transverse diameter; LD, longitudinal diameter; PMC, pericarp moisture content; PP, pericarp proportion; SR, seed yield ratio; PT, pericarp thickness; LC, lignin content; HC, hemicellulose content; CC, cellulose content.

Evolutionary characteristics and structural features of the *CdCSE* gene family

As detailed in the preceding sections, the histological features and cell wall compositions of the *C. drupifera* pericarp undergo significant dynamic changes during development. The deposition of cell wall components, particularly lignin, plays a key role in these processes; it significantly influences the thickness of the pericarp cell wall and exhibits a significant positive correlation with pericarp thickness. Furthermore, our previous transcriptome and metabolome analyses revealed that the significant accumulation of S-lignin is positively correlated with pericarp thickening, during which the upregulated expression of *CSE* directs the metabolic flux, leading to a predominance of S-lignin monomers in thicker pericarps[10].

To further explore the evolutionary characteristics and structural features of the *CSE* gene family involved in this critical lignin biosynthesis process, 17 *CdCSE* genes were identified from the transcriptome of *C. drupifera*. The physicochemical properties and secondary structural compositions of these proteins are listed in Supplementary Table S2. The predicted protein lengths ranged from 257 to 455 amino acids, with theoretical molecular weights of 29.2–50.4 kDa and isoelectric points between 5.37 and 9.59. Most of these proteins were predicted to be stable, hydrophilic proteins with relatively high aliphatic indices.

A phylogenetic tree was constructed using MEGA11, based on the CSE protein sequences from *C. drupifera*, *A. thaliana*, and *P. trichocarpa* (Fig. 5a). The CSE proteins were clustered into six distinct groups. The clade containing *AtCSE1*, *PoptrCSE1*, and *PoptrCSE2*, which are known to be involved in lignin biosynthesis, clustered together with *CdCSE4* and *CdCSE5*, suggesting that these genes may play similar conserved roles in the lignin biosynthetic pathway of *C. drupifera*.

Furthermore, the secondary structures of the 17 identified CdCSE proteins were predicted to investigate their structural characteristics (Fig. 5b). The structures were predominantly composed of random coils (44.89%–55.52%) and α-helices (32.54%–46.24%), followed by extended strands (8.87%–18.03%) interspersed throughout the sequences (Supplementary Table S2). As enzymes belonging to the α/β hydrolase superfamily, the abundant α-helices

https://doi.org/10.48130/fra-0026-0005

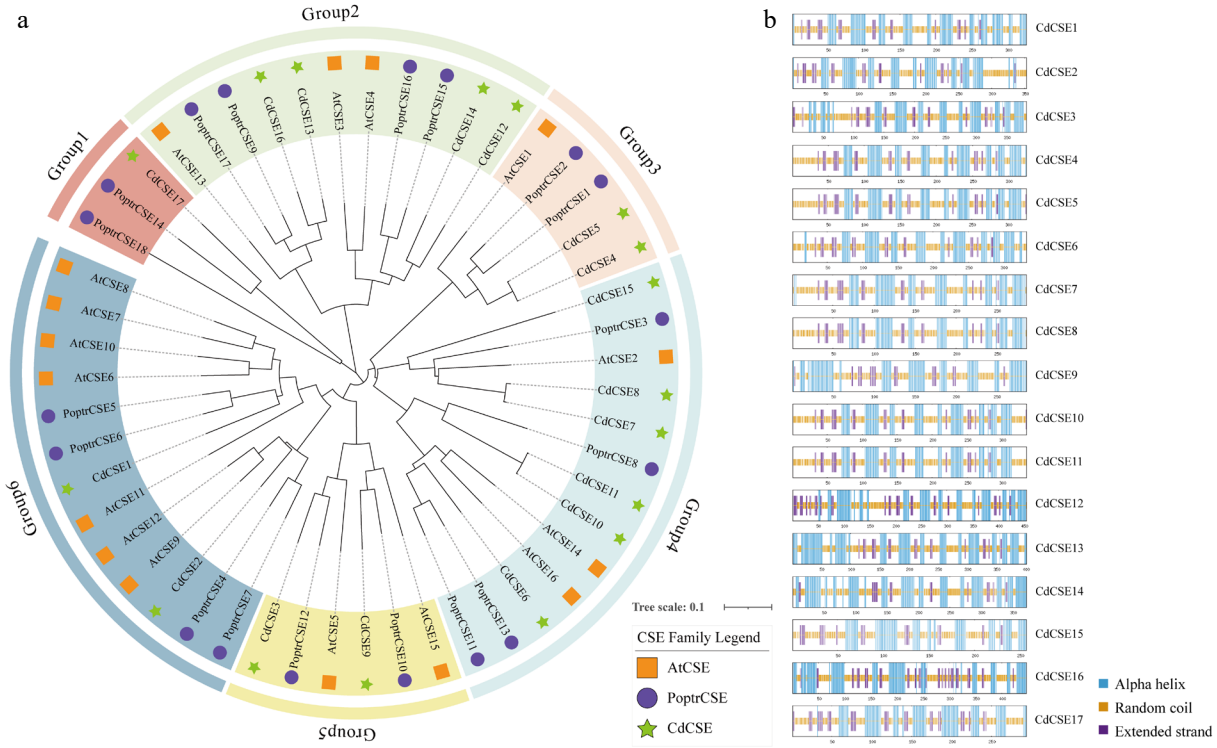

Fig. 5 Evolutionary analysis and secondary structure prediction of the *CdCSE* gene family. (a) Phylogenetic tree of CSE members in *A. thaliana*, *P. trichocarpa*, and *C. drupifera*. (b) Predicted secondary structures of the 17 CdCSE proteins. The colored regions indicate distinct structural elements: Alpha helices (blue), random coils (orange), and extended strands (purple).

provide a stable structural framework, whereas the flexible random coils may form loop regions at the proteins' surface. Additionally, tertiary structure models were generated using the SWISS-MODEL server (Supplementary Fig. S3) to further analyze their spatial conformations. The structural variations, particularly in the flexible coil regions of the 17 members, are likely to influence their distinct substrate-binding affinities and catalytic activities during *C. drupifera*'s growth and development.

Collectively, these findings suggest that the *CdCSE* genes share high evolutionary conservation with their orthologs in other species. The conserved folding patterns and structural variations within the family may influence their specific regulatory functions in lignin biosynthesis and plant development in *C. drupifera*.

Expression profile analysis of *CdCSE* genes in HP and TP pericarp tissues

To further investigate the potential roles of *CdCSE* genes in lignin accumulation during pericarp development, transcriptome data were used to analyze the expression patterns of *CdCSE* genes in HP and TP fruits (Fig. 6). The results showed that most *CdCSE* genes were significantly upregulated during the middle and late developmental stages (S2 and S3) in HP (Fig. 6a). Correlation analysis between gene expression levels and pericarp traits further revealed that *CdCSE2*, *CdCSE4*, *CdCSE5*, *CdCSE6*, and *CdCSE13* were significantly associated with pericarp thickness and lignin content (Fig. 6b). To validate these findings, qRT-PCR analysis was performed on eight representative genes. The results demonstrated that the expression levels of *CdCSE2* and *CdCSE4* were significantly higher in the HP pericarp than in the TP pericarp throughout the developmental process (Fig. 6c). In contrast, *CdCSE13* exhibited a significantly higher expression level in the TP pericarp. Specifically, *CdCSE4* displayed a progressive increase in expression throughout fruit development in HP, whereas its expression remained consistently low in TP pericarps. Given its expression profile and correlation with lignin accumulation, *CdCSE4* was selected for subcellular characterization. Transient expression in epidermal cells of *N. benthamiana* showed that the CdCSE4-GFP protein is distributed within the cytoplasm and at the cell periphery, but is excluded from the nucleus (Supplementary Fig. S4).

CdCSE4 positively regulates lignin biosynthesis and rescues the *cse* mutant phenotype in *A. thaliana*

Compared with the wild type, *CdCSE4*-overexpressing plants (OE#1 and OE#3) exhibited more vigorous growth, with thicker stems and significantly increased plant height. In contrast, the *cse* mutant displayed a stunted phenotype with thinner stems. Notably, the complementation lines expressing *CdCSE4* in the *cse* mutant background largely restored the growth phenotype to the wild-type level (Fig. 7a), indicating that *CdCSE4* can effectively rescue the growth defects of the *cse* mutant. To further investigate the anatomical basis of these phenotypic differences, stem cross-sections were analyzed by phloroglucinol–HCl staining and ultraviolet (UV) autofluorescence (Fig. 7b). Overexpression of *CdCSE4* markedly enhanced lignin deposition in stem tissues, whereas the *cse* mutant exhibited a pronounced reduction in lignification. The complementation (COM) lines restored lignin accumulation to levels similar to those of the wild type.

To further elucidate the role of *CdCSE4* in lignin biosynthesis, the contents of H-, G-, and S-type lignin monomers were quantified in the leaves, stems, and silique pericarps of *A. thaliana* plants across three specific genotypes: Col-0, COM, and OE. As shown in

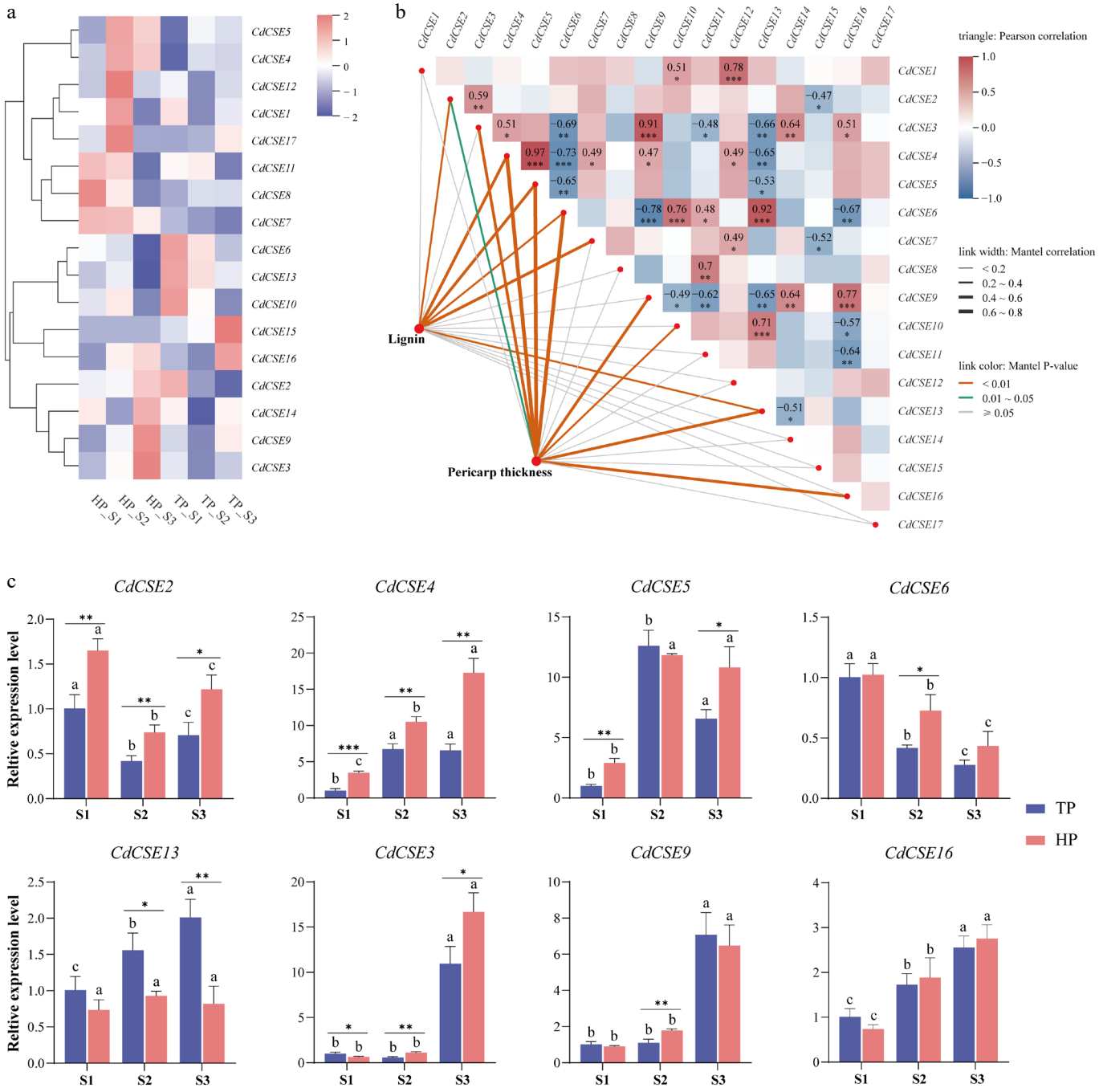

Fig. 6 Expression analysis of *CdCSE* genes in HP and TP pericarps. (a) Heatmap showing the transcriptome expression profiles of *CdCSE* genes at different developmental stages (S1–S3) of HP and TP pericarps. (b) Correlation analysis (Mantel test) of *CdCSE* gene expression levels, lignin content, and pericarp thickness. Edge width indicates Mantel's *r* statistic, and edge color indicates the statistical significance. (c) qRT-PCR validation of eight representative *CdCSE* genes. Error bars represent the standard deviation of three biological replicates. Different letters indicate significant differences between developmental stages within the same pericarp type ($p < 0.05$); asterisks indicate significant differences between HP and TP at the same developmental stage (*** $p < 0.001$; ** $p < 0.01$; * $p < 0.05$).

Fig. 7c, *CdCSE4* overexpression significantly increased the total monolignol content across all tissues. In addition, the monomer composition was altered: The content of H-type lignin increased markedly in leaves and silique pericarps, whereas G-type lignin decreased significantly in silique pericarps. In the complementation lines, H- and G-type lignin levels in leaves decreased, whereas G-type lignin in silique pericarps and S-type lignin in stems increased significantly, with the other components returning to wild-type levels.

Discussion

This study systematically investigated the structural characteristics and molecular mechanisms of pericarp lignification in *C. drupifera*. Through observation of the entire developmental cycle, we found that HP fruits exhibited a significantly higher pericarp proportion, thereby severely limiting the fresh fruits' seed yield. This aligns with previous studies on *Camellia* species, which demonstrated a negative correlation between pericarp thickness and seed

https://doi.org/10.48130/fra-0026-0005

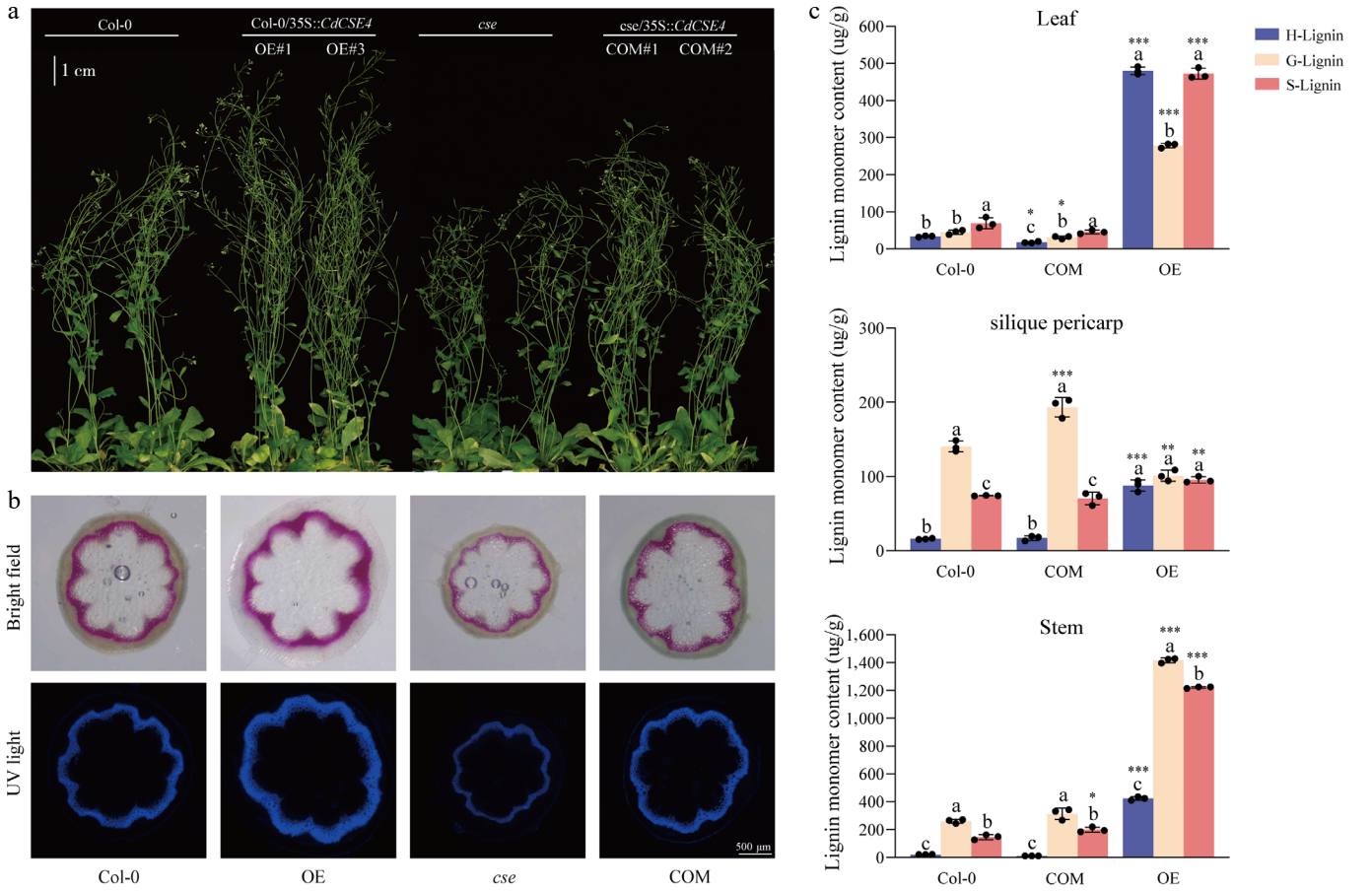

Fig. 7 Functional validation of *CdCSE4* in *A. thaliana* through phenotypic and biochemical analyses. (a) Phenotypic observation of *A. thaliana* wild-type (Col-0), Col-0/35S::*CdCSE4* overexpression lines (OE), *cse* mutant, and *cse*/35S::*CdCSE4* complementation lines (COM). OE#1 and OE#3, alongside COM#1 and COM#2, are the independent transgenic lines used. (b) Phloroglucinol–HCl staining and UV autofluorescence of stem cross-sections from Col-0, OE, *cse*, and COM lines. (c) Comparison of H-, G-, and S-type lignin monomer contents in the leaves, silique pericarps, and stems of different *Arabidopsis* genotypes. Data are presented as the means ± SD (n = 3). Different letters indicate significant differences among the three lignin monomer types (H, G, and S) within the same genotype ($p < 0.05$); asterisks indicate significant differences between the different genotypes and the wild-type Col-0 for the same monomer (*** $p < 0.001$; ** $p < 0.01$; * $p < 0.05$).

yield ratio[30–32]. Paraffin section analysis revealed that, compared with TP fruits, the HP pericarp displayed a markedly higher degree of lignification and thicker cell walls. SEM observations indicated that this was primarily driven by the lamellar accumulation of secondary wall materials, aligning with findings in common *C. oleifera* cultivars[33]. Quantitative analysis of the cell wall components demonstrated that the lignin content in HP was significantly higher than that in TP, exhibiting a strong positive correlation with pericarp thickness. Given that previous studies have confirmed the critical role of the *CSE* gene in S-lignin accumulation in *C. drupifera*[10], we identified 17 highly conserved *CdCSE* genes through genome-wide analysis. Expression profiling also established *CdCSE4* as a key regulatory factor in pericarps' lignin accumulation. Functional validation demonstrated that *CdCSE4* successfully restored the wild-type phenotype in the *A. thaliana cse* mutant, significantly increased total lignin biosynthesis, and altered the proportional composition of lignin monomers.

Pericarp development and lignification in *C. drupifera* represent a continuous spatiotemporal process highly coordinated with seed development. Following pollination and fertilization (November to January), the zygote enters dormancy[34]. Between March and May, ovary wall cells divide rapidly to form the exocarp, mesocarp, and endocarp, as rising temperatures trigger zygotic differentiation into distinct cell lineages[35]. Concurrently, procambium-driven secondary growth and initial lignin deposition commence. Early and robust lignification establishes a rigid physical barrier against pathogen invasion[36,37]. Crucially, complete pericarp lignification serves as both an ecological defense and a developmental safety signal[38]. Rapid seed expansion, initially driven by liquid nutrient accumulation, strictly follows the completion of pericarp lignification[39]. Subsequently, seed coat lignification marks the true initiation of kernel development[40]. Upon its completion, fruit size becomes fixed, pericarp growth ceases, and the kernel enters a phase of massive lipid accumulation[41]. This developmental axis reflects a fundamental shift in metabolic flux within the fruit[42].

During the seed expansion period from May to August, pericarp lignin continues to accumulate. Notably, the allocation of photosynthetic nonstructural carbohydrates to the pericarp during this stage exceeds even that to the leaves and kernels[43,44]. In the later stages of development, sucrose imported into the pericarp is cleaved into fructose and glucose to sustain continuous pericarp thickening and lignification, thereby triggering fierce nutrient competition with the kernel. This source–sink competition indirectly results in the undesirable agronomic trait of large fruit with a thick pericarp that is observed in *C. drupifera* production[45]. However, upon the completion of seed coat lignification, the carbon flux is redirected towards

lipid metabolism in the kernel. Given that lignin biosynthesis is highly carbon-intensive[46], timely attenuation of pericarp lignification during the seed expansion phase could effectively restrict the redundant allocation of carbon to the secondary cell wall. Redirecting these carbon resources to the kernel would greatly optimize source–sink dynamics[47]. This mechanism not only elucidates the principles of metabolic coordination during fruit development but also provides a highly promising molecular breeding strategy to significantly enhance seed yield by downregulating the pericarp's lignification network.

The final thickness of the pericarp is typically determined by a combination of an increased number of cell layers, cell enlargement, and secondary cell wall thickening. In crops such as tomato[48], maize (*Zea mays*)[49], and pepper (*C. annuum*)[9], varieties with thick pericarps possess significantly more cell layers than those with thin pericarps, a process regulated by various phytohormones[50–52]. Following the establishment of cell layers, secondary wall thickening and sclereid formation become the direct driving forces for the pericarp's expansion. Consistent with this, our observations at maturity revealed that both cell wall thickness and sclereid abundance were significantly greater in HP than in TP. Lignin accumulation directly induces cell wall thickening and sclereid formation in the pericarp[33,53,54]. Furthermore, the distribution of sclereids varies across different pericarp layers; the exocarp primarily consists of parenchyma cells, whereas sclereid density progressively increases from the mesocarp to the endocarp[12,55,56], further corroborating our histological findings.

In the lignin biosynthetic pathway, CSE catalyzes the conversion of caffeoyl shikimate into caffeic acid and shikimate. Its biological function has been extensively validated across multiple species. For instance, the *A. thaliana cse* mutant exhibits reduced lignin deposition enriched with *p*-hydroxyphenyl units[16], and a fourfold increase in the conversion rate of cellulose to glucose, leading to collapsed vascular bundles and impaired development[57]. Similar developmental defects and altered lignin profiles have been observed in the *Medicago truncatula cse* mutant[17] and the *Petunia ir-PhCSE* line[19]; overexpression of *PbCSE1* in pear increased the lignin content[18]. The present study marks the first functional characterization of a *CSE* gene (*CdCSE4*) in the genus *Camellia*, demonstrating that its overexpression significantly enhances lignin biosynthesis, alters the proportion of monomers, and successfully restores the wild-type phenotype in the *Arabidopsis* mutant. Upstream of these biosynthetic genes, transcription factors (particularly MYB family members such as MYB46 and MYB83) act as master regulators, activating genes including *CSE*, *COMT*, *CCR*, and *CAD*[57]. In woody plants, transcription factors such as PbrMYB169 in pear[58], CsMYB85 in citrus[59], and PtrMYB152 in poplar[60] have been shown to regulate secondary wall formation and lignin biosynthesis. Collectively, these studies suggest that the expression of *CdCSE4* is highly likely to be finely tuned by a complex MYB-mediated regulatory network, although the specific interaction mechanisms of the transcription factors in *Camellia* warrant further investigation.

Although this study provides comprehensive insights into the lignification process, certain limitations must be acknowledged. First, our research primarily focused on the impact of secondary wall thickening on pericarp thickness, without delving deeply into cells' division and expansion during the primary growth phase of the cell wall. Therefore, future research should aim to establish a coordinated, continuous regulatory model encompassing the process of cell layer proliferation → cell expansion → lignification (cell wall thickening) to fully elucidate the ontogeny of the pericarp. Second, constrained by the current technical bottlenecks in the genetic transformation of woody plants, the functional validation of *CdCSE4* was performed in the herbaceous model plant *A. thaliana*. Establishing a stable genetic transformation system for *C. drupifera* is a critical next step. Overcoming this hurdle will enable the in vivo regulation of metabolic flux, thereby facilitating the breeding of elite *Camellia* cultivars characterized by large fruits, thin pericarps, and a high oil content.

Conclusions

This study elucidates the structural characteristics and molecular regulatory mechanisms of pericarp lignification in *C. drupifera* by systematically constructing a spatiotemporal dynamic map spanning the entire 311-d developmental cycle. Histological analysis revealed that pericarp lignification initiates early in development (124–168 d), progressing from the exocarp to the endocarp. This establishes that secondary wall thickening and sclereid development form the structural basis underlying the HP phenotype. Quantification of the cell walls' components confirmed that substantial lignin deposition exhibits a strong positive correlation with both cell wall thickness and overall pericarp thickness. Furthermore, the *CdCSE* gene family was identified in *C. drupifera* for the first time. Expression profiling highlighted *CdCSE4* as a core regulatory gene in lignin biosynthesis in the pericarp. It rescues the growth phenotype of lignin-deficient mutants and positively regulates total lignin biosynthesis and the proportional composition of its monomers. In conclusion, this study unveils the dynamic principles and molecular regulatory basis of pericarp lignification in *C. drupifera*, providing theoretical insights and valuable candidate gene resources for optimizing pericarp structure, increasing seed yield, and improving seed oil quality.

Author contributions

The authors confirm their contributions to the paper as follows: study conception and design, funding acquisition: Liao B, Li Y (Yongquan Li); methodology: Liao B, Zhang B; formal analysis, draft manuscript preparation: Shen Y; data curation: Shen Y, Xiong W; investigation: Xiong W, He S, Shen H, Li Y (Yongjuan Li); writing – review and editing: Liao B, Shen Y; supervision: Li Y (Yongquan Li). All authors reviewed the results and approved the final version of the manuscript.

Data availability

The data that support the findings of this study are available from the corresponding author upon reasonable request.

Acknowledgments

This research was supported by the Forestry Science and Technology Innovation Projects of Guangdong Province (2024KJCX004, 2023KJCX006) and the Science and Technology Plan Project of Meizhou City (2025A03032001). The authors gratefully acknowledge the ZHKU-Huizhou Seed-oil Camellia Science and Technology Backyard for providing the plant materials used in this study.

Conflict of interest

The authors declare that they have no conflict of interest.

Supplementary information accompanies this paper online at: https://doi.org/10.48130/fra-0026-0005.

https://doi.org/10.48130/fra-0026-0005

Dates

Received 29 January 2026; Revised 15 April 2026; Accepted 20 April 2026; Published online 24 July 2026

References

[1] Hu Z, Yang K, Yu A. 2025. The extraction technologies, nutritional compositions, and health benefits of *Camellia oleifera* seed oil—a review. *Journal of Oleo Science* 74:859–878

[2] Xu P, Cai Y, Chen K, You R, Lu Y. 2026. *Camellia oleifera* oil: unveiling health benefits and exploring novel applications. *Critical Reviews in Food Science and Nutrition* 66:108–128

[3] Gao S, Wang B, Liu F, Zhao J, Yuan J, et al. 2022. Variation in fruit morphology and seed oil fatty acid composition of *Camellia oleifera* collected from diverse regions in Southern China. *Horticulturae* 8:818

[4] Zheng S, Kong Q, Yan H, Liu J, Tang R, et al. 2025. Phenotypic diversity analysis and integrative evaluation of *Camellia oleifera* germplasm resources in Ya'an, Sichuan Province. *Plants* 14:2249

[5] Yang L, Gao C, Wei H, Long L, Qiu J. 2022. Evaluation of the economic characteristics of the fruit of 45 superior *Camellia weiningensis* Y.K. Li. trees. *PLoS One* 17:e0268802

[6] Song W, Huang S, Li F, Tu P, Li Y, et al. 2025. Selection and preliminary evaluation of superior individual plant in *Camellia oleifera*. *PeerJ* 13:e20283

[7] Shen H, Liao B, Deng J, Liu B, Shen Y, et al. 2024. Transcriptome analysis of multiple plant parts in the woody oil tree *Camellia drupifera* loureiro. *Horticulturae* 10:914

[8] Zhong R, Ye ZH. 2015. Secondary cell walls: biosynthesis, patterned deposition and transcriptional regulation. *Plant & Cell Physiology* 56:195–214

[9] Gong C, Zeng M, Guo G, Pan B, Gao C, et al. 2025. Integrated analysis of dynamic changes in cell wall components and transcriptome profiles during pepper pericarp development. *Scientia Horticulturae* 352:114443

[10] Li Y, Liao B, Wang Y, Luo H, Wang S, et al. 2022. Transcriptome and metabolome analyses provide insights into the relevance of pericarp thickness variations in *Camellia drupifera* and *Camellia oleifera*. *Frontiers in Plant Science* 13:1016475

[11] Vicente-Flores M, Güemes-Vera N, Chanona-Pérez JJ, Perea-Flores MJ, Arzate-Vázquez I, et al. 2021. Study of cellular architecture and micromechanical properties of cuajilote fruits (*Parmentiera edulis* D. C.) using different microscopy techniques. *Microscopy Research and Technique* 84:12–27

[12] Wang Q, Hu J, Yang T, Chang S. 2021. Anatomy and lignin deposition of stone cell in *Camellia oleifera* shell during the young stage. *Protoplasma* 258:361–370

[13] Xu M, He S, Zhang H, Gao S, Yin M, et al. 2025. Gibberellin regulates the synthesis of stone cells in 'Nanguo' pear via the *PuMYB91-PuERF023* module. *Physiologia Plantarum* 177:e70074

[14] Zhang H, Gao S, Wang T, Xu M, Li X, et al. 2022. Ca^{2+} mediates transcription factor *PuDof2.5* and suppresses stone cell production in pear fruits. *Frontiers in Plant Science* 13:976977

[15] Boerjan W, Ralph J, Baucher M. 2003. Lignin biosynthesis. *Annual Review of Plant Biology* 54:519–546

[16] Vanholme R, Cesarino I, Rataj K, Xiao Y, Sundin L, et al. 2013. Caffeoyl shikimate esterase (CSE) is an enzyme in the lignin biosynthetic pathway in *Arabidopsis*. *Science* 341:1103–1106

[17] Ha CM, Escamilla-Trevino L, Serrani Yarce JC, Kim H, Ralph J, et al. 2016. An essential role of caffeoyl shikimate esterase in monolignol biosynthesis in *Medicago truncatula*. *The Plant Journal* 86:363–375

[18] Xu J, Tao X, Xie Z, Gong X, Qi K, et al. 2021. *PbCSE1* promotes lignification during stone cell development in pear (*Pyrus bretschneideri*) fruit. *Scientific Reports* 11:9450

[19] Kim JY, Cho KH, Keene SA, Colquhoun TA. 2023. Altered profile of floral volatiles and lignin content by down-regulation of *Caffeoyl Shikimate Esterase* in Petunia. *BMC Plant Biology* 23:210

[20] Wang X, Chao N, Zhang A, Kang J, Jiang X, et al. 2021. Systematic analysis and biochemical characterization of the caffeoyl shikimate esterase gene family in poplar. *International Journal of Molecular Sciences* 22:13366

[21] Yu Y, He J, Liu L, Zhao H, Zhang M, et al. 2023. Characterization of caffeoyl shikimate esterase gene family identifies *CsCSE5* as a positive regulator of *Podosphaera xanthii* and *Corynespora cassiicola* pathogen resistance in cucumber. *Plant Cell Reports* 42:1937–1950

[22] Ye H, Gao H, Li J, Lu L, Zheng S, et al. 2025. Mitigating response of *SlCSE06* induced by 2-ethylfuran to *Botrytis cinerea* infection. *Plants* 14:575

[23] Pradhan Mitra P, Loqué D. 2014. Histochemical staining of *Arabidopsis thaliana* secondary cell wall elements. *Journal of Visualized Experiments* 87:e51381

[24] Lin CC, Kao CH. 2001. Cell wall peroxidase against ferulic acid, lignin, and NaCl-reduced root growth of rice seedlings. *Journal of Plant Physiology* 158:667–671

[25] Lu F, Ralph J. 1997. Derivatization followed by reductive cleavage (DFRC method), a new method for lignin analysis: protocol for analysis of DFRC monomers. *Journal of Agricultural and Food Chemistry* 45:2590–2592

[26] Lin P, Wang K, Wang Y, Hu Z, Yan C, et al. 2022. The genome of oil-Camellia and population genomics analysis provide insights into seed oil domestication. *Genome Biology* 23:14

[27] Mistry J, Chuguransky S, Williams L, Qureshi M, Salazar GA, et al. 2021. Pfam: the protein families database in 2021. *Nucleic Acids Research* 49:D412–D419

[28] Chen C, Wu Y, Li J, Wang X, Zeng Z, et al. 2023. TBtools-II: a "one for all, all for one" bioinformatics platform for biological big-data mining. *Molecular Plant* 16:1733–1742

[29] Tamura K, Stecher G, Kumar S. 2021. MEGA11: molecular evolutionary genetics analysis version 11. *Molecular Biology and Evolution* 38:3022–3027

[30] Yang L, Gao C, Xie J, Qiu J, Deng Q, et al. 2022. Fruit economic characteristics and yields of 40 superior *Camellia oleifera* Abel plants in the low-hot valley area of Guizhou Province, China. *Scientific Reports* 12:7068

[31] Sun D, Gao C, Song Q, Wan X, Wang Q, et al. 2026. Analysis and evaluation of fruit traits of wild *Camellia oleifera* germplasm in the high-altitude region of Northwest Guizhou, China. *New Forests* 57:13

[32] Zhao J. 2021. *Evaluation of Main Characters and Screening of Superior Trees of Camellia gauchowensis Chang in Jieyang, Guangdong Province*. Thesis. Central South University of Forestry and Technology, China. pp. 10–57 (in Chinese) doi: 10.27662/d.cnki.gznlc.2021.000380

[33] Xiang X. 2023. *Changes of pericarp development and contents of Camellia oleifera*. Thesis. Central South University of Forestry and Technology, China. pp. 7–55 (in Chinese) doi: 10.27662/d.cnki.gznlc.2023.001538

[34] Gao C, Yuan D, Yang Y, Wang B, Liu D, et al. 2015. Pollen tube growth and double fertilization in *Camellia oleifera*. *Journal of the American Society for Horticultural Science* 140:12–18

[35] Zhao S, Rong J. 2024. Single-cell RNA-seq reveals a link of ovule abortion and sugar transport in *Camellia oleifera*. *Frontiers in Plant Science* 15:1274013

[36] Bhuiyan NH, Selvaraj G, Wei Y, King J. 2009. Role of lignification in plant defense. *Plant Signaling & Behavior* 4:158–159

[37] Miedes E, Vanholme R, Boerjan W, Molina A. 2014. The role of the secondary cell wall in plant resistance to pathogens. *Frontiers in Plant Science* 5:358

[38] Radchuk V, Borisjuk L. 2014. Physical, metabolic and developmental functions of the seed coat. *Frontiers in Plant Science* 5:510

[39] Weber H, Borisjuk L, Wobus U. 2005. Molecular physiology of legume seed development. *Annual Review of Plant Biology* 56:253–279

[40] Debeaujon I, Léon-Kloosterziel KM, Koornneef M. 2000. Influence of the testa on seed dormancy, germination, and longevity in *Arabidopsis*. *Plant Physiology* 122:403–414

[41] Baud S, Lepiniec L. 2010. Physiological and developmental regulation of seed oil production. *Progress in Lipid Research* 49:235–249

[42] Allen DK, Young JD. 2013. Carbon and nitrogen provisions alter the metabolic flux in developing soybean embryos. *Plant Physiology* 161:1458–1475

[43] Shen CH, Chen RF, Liu Z, Xi RC. 2024. Characteristics of the transport and distribution of photosynthetic products during fruit expansion of *Camellia gauchowensis*. *Journal of Central South University of Forestry & Technology* 44:58–66 (in Chinese)

[44] Li Y, Xie Y, Zhang Y, Fang X, Wang J. 2025. Trade-offs and partitioning strategy of carbon source-sink during fruit development of *Camellia oleifera*. *Plants* 14:1920

[45] Liu Z, Shen C, Chen R, Fu Z, Deng X, et al. 2024. Combination of transcriptomic, biochemical, and physiological analyses reveals sugar metabolism in *Camellia drupifera* fruit at different developmental stages. *Frontiers in Plant Science* 15:1424284

[46] Amthor JS. 2003. Efficiency of lignin biosynthesis: a quantitative analysis. *Annals of Botany* 91:673–695

[47] Novaes E, Kirst M, Chiang V, Winter-Sederoff H, Sederoff R. 2010. Lignin and biomass: a negative correlation for wood formation and lignin content in trees. *Plant Physiology* 154:555–561

[48] Gan L, Song M, Wang X, Yang N, Li H, et al. 2022. Cytokinins are involved in regulation of tomato pericarp thickness and fruit size. *Horticulture Research* 9:uhab041

[49] Gong G, Jia H, Tang Y, Pei H, Zhai L, et al. 2024. Genetic analysis and QTL mapping for pericarp thickness in maize (*Zea mays* L.). *BMC Plant Biology* 24:338

[50] Zhu Z, Liang H, Chen G, Li F, Wang Y, et al. 2019. The bHLH transcription factor *SlPRE2* regulates tomato fruit development and modulates plant response to gibberellin. *Plant Cell Reports* 38:1053–1064

[51] Xiong C, Pei H, Zhang Y, Ren W, Ma Z, et al. 2022. Integrative analysis of transcriptome and miRNAome reveals molecular mechanisms regulating pericarp thickness in sweet corn during kernel development. *Frontiers in Plant Science* 13:945379

[52] Liu X, Chen Y, Yuan B, Peng M, Zhao Y, et al. 2025. Identification of the citrus GRF gene family and its expression in fruit peel thickening mediated by gibberellin. *BMC Plant Biology* 25:216

[53] Jin Q, Yan C, Qiu J, Zhang N, Lin Y, et al. 2013. Structural characterization and deposition of stone cell lignin in Dangshan Su pear. *Scientia Horticulturae* 155:123–130

[54] Dardick C, Callahan AM. 2014. Evolution of the fruit endocarp: molecular mechanisms underlying adaptations in seed protection and dispersal strategies. *Frontiers in Plant Science* 5:284

[55] Cerri M, Reale L. 2020. Anatomical traits of the principal fruits: an overview. *Scientia Horticulturae* 270:109390

[56] Khan MKU, Muhammad N, Jia Z, Peng J, Liu M. 2022. Mechanism of stone (hardened endocarp) formation in fruits: an attempt toward pitless fruits, and its advantages and disadvantages. *Genes* 13:2123

[57] Vargas L, Cesarino I, Vanholme R, Voorend W, de Lyra Soriano Saleme M, et al. 2016. Improving total saccharification yield of Arabidopsis plants by vessel-specific complementation of *caffeoyl shikimate esterase* (*cse*) mutants. *Biotechnology for Biofuels* 9:139

[58] Xue C, Yao JL, Xue YS, Su GQ, Wang L, et al. 2019. *PbrMYB169* positively regulates lignification of stone cells in pear fruit. *Journal of Experimental Botany* 70:1801–1814

[59] Jia N, Liu J, Tan P, Sun Y, Lv Y, et al. 2019. *Citrus sinensis* MYB transcription factor *CsMYB85* induce fruit juice sac lignification through interaction with other *CsMYB* transcription factors. *Frontiers in Plant Science* 10:213

[60] Wang S, Li E, Porth I, Chen JG, Mansfield SD, et al. 2014. Regulation of secondary cell wall biosynthesis by poplar R2R3 MYB transcription factor PtrMYB152 in *Arabidopsis*. *Scientific Reports* 4:5054